

Cytochrome *c'* folding triggered by electron transfer: Fast and slow formation of four-helix bundles

Jennifer C. Lee, Harry B. Gray, and Jay R. Winkler*

Beckman Institute, MC 139-74, California Institute of Technology, Pasadena, CA 91125-7400

Contributed by Harry B. Gray, May 11, 2001

Reduced (Fe^{II}) *Rhodopseudomonas palustris* cytochrome *c'* (Cyt *c'*) is more stable toward unfolding ([GuHCl]_{1/2} = 2.9(1) M) than the oxidized (Fe^{III}) protein ([GuHCl]_{1/2} = 1.9(1) M). The difference in folding free energies ($\Delta\Delta G_f^\circ = 70$ meV) is less than half of the difference in reduction potentials of the folded protein (100 mV vs. NHE) and a free heme in aqueous solution (≈ -150 mV). The spectroscopic features of unfolded Fe^{II}-Cyt *c'* indicate a low-spin heme that is axially coordinated to methionine sulfur (Met-15 or Met-25). Time-resolved absorption measurements after CO photodissociation from unfolded Fe^{II}(CO)-Cyt *c'* confirm that methionine can bind to the ferroheme on the microsecond time scale [$k_{\text{obs}} = 5(2) \times 10^4$ s⁻¹]. Protein folding was initiated by photoreduction (two-photon laser excitation of NADH) of unfolded Fe^{III}-Cyt *c'* ([GuHCl] = 2.02–2.54 M). Folding kinetics monitored by heme absorption span a wide time range and are highly heterogeneous; there are fast-folding ($\approx 10^3$ s⁻¹), intermediate-folding (10^2 – 10^1 s⁻¹), and slow-folding (10^{-1} s⁻¹) populations, with the last two likely containing methionine-ligated (Met-15 or Met-25) ferrohemes. Kinetics after photoreduction of unfolded Fe^{III}-Cyt *c'* in the presence of CO are attributable to CO binding [$1.4(6) \times 10^3$ s⁻¹] and Fe^{II}(CO)-Cyt *c'* folding [$2.8(9)$ s⁻¹] processes; stopped-flow triggered folding of Fe^{III}-Cyt *c'* (which does not contain a protein-derived sixth ligand) is adequately described by a single kinetics phase with an estimated folding time constant of ≈ 4 ms [$\Delta G_f^\circ = -33(3)$ kJ mol⁻¹] at zero denaturant.

Energy-landscape descriptions of protein folding emphasize the roles of free energy and energy-surface ruggedness as key determinants of folding dynamics (1–3). The many correlations of folding times with free energy support this point of view, but it is difficult to reconcile the model with the seemingly simple kinetics that often are observed. Analyses of experimental data point to a relationship between the folding kinetics and the topology of the native protein structure (4–8). Proteins that, on average, have a large number of long-range contacts in the folded state tend to fold more slowly than those with a preponderance of short-range contacts. The questions remain: is it the depth and roughness of the funnel, the topology of the folded state, or some combination of the two that determines the folding mechanism?

Short-range contacts outnumber long-range interactions in helical bundles; if topology is the key, then these proteins should fold rapidly (4, 5). Highly helical ferrocycytochrome *b*₅₆₂ (Fe^{II}-Cyt *b*₅₆₂) (9, 10), acyl-CoA binding protein (ACBP) (11–14), the E colicin binding immunity proteins Im7 and Im9 (15, 16), and the N-terminal domain of phage λ repressor (17) all fold on the millisecond time scale. These observations appear to support the notion that folded-state structural topology is of central importance in folding dynamics and that helical bundle structures are inherently fast folding.

We have shown previously that Fe^{II}-Cyt *b*₅₆₂ folding can be triggered by electron transfer (ET), a method that takes advantage of the greater stabilities of reduced heme proteins in native states (9, 10, 18, 19). Although folded Fe^{II}-Cyt *b*₅₆₂ was observed within milliseconds after reduction of the unfolded oxidized protein, no more than half of the reduced protein successfully developed native structure (10). Rapid heme dissociation from

the polypeptide ($k_{\text{diss}} \approx 2\text{--}7 \times 10^3$ s⁻¹) limited the yield of the folding reaction. The heme-loss step selects fast-folding conformations from the unfolded ensemble; if there are slow-folding components, they cannot be detected. Under these circumstances, the observed kinetics reflect heme-dissociation dynamics rather than folding.

Cytochrome *c'* (Cyt *c'*) from the photosynthetic bacterium *Rhodopseudomonas palustris* is a monomeric, soluble, 125-residue, four-helix-bundle heme protein. Importantly, the porphyrin is bound to the polypeptide with two thioether links near the C terminus (Cys-113 and Cys-116) (20–22). Although sharing just 19% sequence identity and 40% similarity (23), Cyt *c'* and Cyt *b*₅₆₂ have quite similar folds (1.6-Å rms deviation in α -carbon position) (Fig. 1) (24, 25). Cyt *b*₅₆₂ has a six-coordinate, low-spin heme with Met-7 and His-102 axial ligands [^(H102N){PorN₄Fe^{III}}(M⁷S)⁺] and a reduction potential of 180 mV vs. NHE (24, 26). Cyt *c'* has a high-spin, five-coordinate heme, axially ligated by His-117 [^(H117N){PorN₄Fe^{III}}]⁺ and a reduction potential of 100 mV (27–32). In Cyt *c'*, the side-chain of Leu-12 fills the space occupied by a sixth ligand in Cyt *b*₅₆₂ (Fig. 1 *Inset*) (25); movement of this bulky group is necessary for ligand binding.

The Fe^{III/II} reduction potential is high enough to permit ET triggering of Fe^{II}-Cyt *c'* folding in the 2.0–2.9 M guanidine hydrochloride (GuHCl) concentration range. Fe^{II}-Cyt *c'* folding is highly heterogeneous, spanning a time range from milliseconds to several seconds. Importantly, the folding kinetics of Fe^{III}-Cyt *c'* and Fe^{II}(CO)-Cyt *c'* are less complex, indicating that nonnative ligand traps may be responsible for the complexity of Fe^{II}-Cyt *c'* folding.

Materials and Methods

GuHCl (Sigma, ultrapure grade), Tris(2,2'-bipyridine)ruthenium(II) chloride ([Ru(bpy)₃]Cl₂, Strem), and NADH (Sigma) were used as received.

Spectroscopic measurements were made as follows: absorption, Hewlett-Packard 8452 diode array spectrophotometer; CD, Aviv 62ADS spectropolarimeter; and luminescence, Hitachi F-4500 spectrofluorimeter ($\lambda_{\text{ex}} = 290$ nm; $\lambda_{\text{obsd}} = 300$ – 500 nm). Mass spectral analyses were done at the Protein/Peptide Microanalytical Laboratory in the Beckman Institute at Caltech.

R. palustris strain 37 (ATCC 17007) Cyt *c'* was isolated and purified by using minor modifications of published procedures (31, 33). Cyt *c'* was chromatographed either on a CM Sepharose column equilibrated with 5 mM sodium phosphate and 10 mM NaCl (pH 7.0) in the presence of ferricyanide and eluted with the charging buffer, or on a column of hydroxyapatite (type I, Bio-Rad) equilibrated with 3 mM sodium phosphate and 15 mM NaCl (pH 7.0) in the presence of mercaptoethanol and eluted

Abbreviations: Cyt *b*₅₆₂, cytochrome *b*₅₆₂; ACBP, acyl-CoA binding protein; Im, E colicin binding immunity protein; Cyt *c'*, cytochrome *c'*; ET, electron transfer; GuHCl, guanidine hydrochloride; bpy, 2,2'-bipyridine.

*To whom reprint requests should be addressed. E-mail: winklerj@caltech.edu.

The publication costs of this article were defrayed in part by page charge payment. This article must therefore be hereby marked "advertisement" in accordance with 18 U.S.C. §1734 solely to indicate this fact.

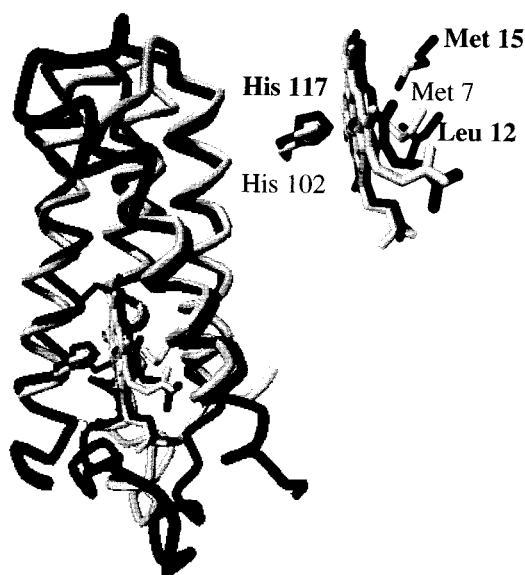


Fig. 1. Comparison of heme environments. In Cyt b_{562} (gray), the heme iron is axially ligated to His-102 and Met-7, whereas in Cyt c' (black), the heme has only one axial ligand (His-117) with the side chain of Leu-12 at the other axial site. The nearest methionine residue (Met-15) in Cyt c' is also shown. Backbone atoms of four α -helices of Cyt c' (PDB 1A7V) are superimposed on the corresponding atoms in Cyt b_{562} (PDB 256B), with a calculated rms deviation of 1.6 Å.

with a linear gradient from 10 mM to 100 mM sodium phosphate buffer (15 mM NaCl, pH 7.0). Proteins used in all experiments had purity indices ($A_{280\text{ nm}}/A_{398\text{ nm}}$, oxidized) between 0.22 and 0.25 (literature value, 0.21) (33). Although only a single fraction was isolated chromatographically, mass spectra revealed two components in the protein sample. The mass of one component matched that expected on the basis of the amino acid sequence (13,748 daltons); the other had a mass 17 atomic mass units lower than predicted. Protein concentrations were obtained from UV-visible absorption measurements (Fe^{III}-Cyt c' , $\epsilon_{398\text{ nm}} = 85\text{ mM}^{-1}\text{cm}^{-1}$; Fe^{II}-Cyt c' , $\epsilon_{426\text{ nm}} = 99\text{ mM}^{-1}\text{cm}^{-1}$) (34). GuHCl concentrations were extracted from refractive index determinations (Abbe-3L refractometer, Milton Roy, Rochester, NY) (35).

Denaturation curves for Fe^{II}-Cyt c' were determined in the presence of excess sodium dithionite. Transient absorption spectra and kinetics were measured by using an apparatus described previously (36). The excitation source was the third harmonic of a Q-switched Nd:YAG laser (355 nm) for electron photoinjection from NADH, and a Nd:YAG pumped optical parametric oscillator (480 nm) for injection from Ru(bpy)₃²⁺ and for CO photolysis experiments. A 16-bit, 20 MS/s digital oscilloscope (CompuScope 1602, Gage Applied) was used to record the complete kinetics traces from 10⁻³ to 10¹ s. Samples for kinetics measurements were deoxygenated by repeated evacuation/argon-fill cycles on a Schlenk line. Typical samples contained Cyt c' (100–200 μM), either Ru(bpy)₃²⁺ (1.0–1.5 equivalents) or NADH (2.0–2.5 equivalents), and GuHCl (1.8–3.5 M) in 100 mM sodium phosphate buffer (pH 7). The pH and index of refraction were measured after laser experiments. Reduced protein was stirred under 1 atm of CO for at least 30 min after deoxygenation to prepare Fe^{II}(CO)-Cyt c' .

Measured kinetics traces were logarithmically compressed (100 points per time decade), normalized [$I(t) - I(t_\infty)/I(t_0) - I(t_\infty)$], and fit by using a non-negative linear least-squares minimization algorithm to project the folding kinetics onto a basis of exponential decay functions with rate constants in the range 10⁵

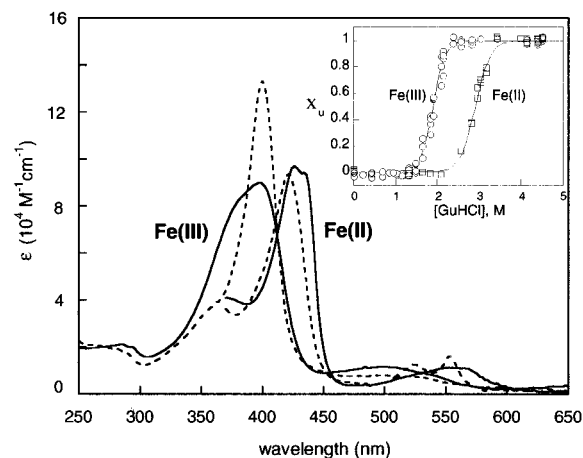


Fig. 2. Absorption spectra of folded Fe^{III}-Cyt c' and Fe^{II}-Cyt c' (bold lines), and unfolded Fe^{III}-Cyt c' and Fe^{II}-Cyt c' (dashed lines). (*Inset*) GuHCl titration curves generated from CD, fluorescence, and Soret absorption data (χ_u is the unfolded-protein fraction).

to 10⁻² s⁻¹ (10 rate constants per decade, spaced logarithmically).

The folding kinetics of Fe^{III}-Cyt c' were measured by using a BioLogic SFM-4S stopped-flow mixer, coupled via optical fiber to a monochromator fitted with a five-stage photomultiplier tube. Probe light was provided by a 200-W Hg/Xe arc lamp. The PMT output was recorded with the 16-bit digital oscilloscope. Kinetics traces were measured at 372 nm (formation of folded protein, $\Delta\epsilon = 28\text{ mM}^{-1}\text{cm}^{-1}$) and 400 nm (disappearance of the unfolded protein, $\Delta\epsilon = -44\text{ mM}^{-1}\text{cm}^{-1}$) for a time period up to 25 s, at a sampling rate of 2 or 5 kS/s. In all refolding experiments, unfolded Fe^{III}-Cyt c' (3.3 M GuHCl) was either diluted 6- or 12-fold with a combination of Hepes buffer ([Hepes] = 0.1 M, pH 7) and Hepes/GuHCl ([Hepes] = 0.1 M, [GuHCl] = 3.3 M, pH 7), giving final protein concentrations of 1.5 μM and varying GuHCl concentrations (0.6–1.80 M). Kinetics traces were fit to single exponential functions.

Results

Equilibrium Unfolding. GuHCl titration curves generated from far-UV CD, Trp-72 fluorescence, and Soret absorbance spectra show that reduced Cyt c' is more stable toward unfolding ($[\text{GuHCl}]_{1/2} = 2.9(1)\text{ M}$) than oxidized Cyt c' ($[\text{GuHCl}]_{1/2} = 1.9(1)\text{ M}$) (Fig. 2 *Inset*). The stability of folded Cyt c' , judged by the folding free-energy change extrapolated to zero denaturant (ΔG_f°), is measurably lower than that of Cyt b_{562} [Fe(III) : $\Delta G_f^\circ(\text{Cyt } c') = -33(3)\text{ kJ mol}^{-1}$, $\Delta G_f^\circ(\text{Cyt } b_{562}) = -42(3)\text{ kJ mol}^{-1}$; Fe(II) : $\Delta G_f^\circ(\text{Cyt } c') = -40(4)\text{ kJ mol}^{-1}$, $\Delta G_f^\circ(\text{Cyt } b_{562}) \approx -78\text{ kJ mol}^{-1}$]. The difference in folding free energies between Fe^{III}- and Fe^{II}-Cyt c' ($\Delta\Delta G_f^\circ = 7\text{ kJ mol}^{-1} \approx 70\text{ meV}$) is less than half that predicted on the basis of the reduction potential of the folded protein (100 mV vs. NHE) and the potential expected for a heme in aqueous solution (-150 mV) (37). The titrations suggest that the potential of the unfolded protein is $\approx 0\text{ V}$, possibly because a second axial ligand binds to the heme when the protein unfolds. Although the difference in folding free energies is smaller than anticipated, it is large enough to permit ET triggering of Fe^{II}-Cyt c' folding between 2 and 2.9 M GuHCl.

Ligand Binding to Unfolded Cyt c' . Addition of GuHCl to solutions of Fe^{III}-Cyt c' narrows the Soret absorption band ($\lambda_{\text{max}} = 400\text{ nm}$, $\epsilon = 133\text{ mM}^{-1}\text{cm}^{-1}$) (Fig. 2). The absorption profile is analogous to that of the M80A mutant of cytochrome c ($\lambda_{\text{max}} = 400\text{ nm}$, $\epsilon = 164\text{ mM}^{-1}\text{cm}^{-1}$, pH = 4.5) (38) and is consistent

with the formation of a six-coordinate, high-spin heme (^{H17}N) $\{^{Por}N_4Fe^{III}\}(OH_2)^+$. The absorption spectrum in alkaline solution (pH > 10, [GuHCl] \geq 3.5 M) is typical of a low-spin Fe^{III} heme ($\lambda_{max} = 406$ nm, $\epsilon = 100$ $mM^{-1}cm^{-1}$) (38); in this case, it is possible that a lysine residue binds to form (^{H17}N) $\{^{Por}N_4Fe^{III}\}(^KN)^+$. Unlike cytochrome *c*, Cyt *c'* has no His residues (other than the native His-117 ligand) available to bind to the Fe^{III} heme in the unfolded protein.

GuHCl denaturation induces a blue shift in the Soret absorption of Fe^{II} -Cyt *c'* (folded: $\lambda_{max} = 426, 435$ nm; unfolded: $\lambda_{max} = 420$ nm), and two sharp Q-bands then appear ($\lambda_{max} = 524, 552$ nm). These spectroscopic features are consistent with a six-coordinate, low-spin heme (Fig. 2). The absence of strongly shifted peaks in the 1H NMR spectrum of unfolded Fe^{II} -Cyt *c'* also signals the presence of a diamagnetic heme. The absorption spectrum of the unfolded Fe^{II} protein is independent of pH in the range 4–10, although changes in Soret absorption at higher pH levels are consistent with lysine binding ($\lambda_{max} = 416, 520, 550$ nm). Addition of *N*-acetyl-L-methionine to unfolded Fe^{II} -Cyt *c'* causes little perturbation of the spectrum, suggesting methionine sulfur coordination [$(^{H17}N)\{^{Por}N_4Fe^{II}\}(^MS)$, Met-15 and/or Met-25] in unfolded Fe^{II} -Cyt *c'*. Methionine binding in unfolded Fe^{II} -Cyt *c'* would raise the reduction potential and could explain the small difference between the folding free-energy changes in Fe^{II} - and Fe^{III} -Cyt *c'*.

Misligated Met residues must dissociate from the heme before Cyt *c'* can adopt its native folded structure. Indeed, the folding dynamics of Fe^{II} -Cyt *c'* could reflect the kinetics of ligand substitutions. We have used two methods to examine the kinetics of MS binding to Fe^{II} in unfolded Cyt *c'*. Laser-excited $Ru(bpy)_3^{2+}$ reduces unfolded Fe^{III} -Cyt *c'* ([GuHCl] = 4.4 M) in less than a microsecond. After the rapid [$1.4(1) \times 10^6$ s^{-1}] change in absorbance corresponding to heme reduction, there is no substantial variation in the spectrum of the reduced protein until charge recombination regenerates unfolded Fe^{III} -Cyt *c'*. The transient difference spectrum recorded 20 μs after the laser flash reveals a mixture of high- and low-spin hemes, suggesting that a nonnative sixth ligand rapidly binds to the heme in the unfolded reduced protein. Ligand binding dynamics also were examined after photodissociation of CO from unfolded $Fe^{II}(CO)$ -Cyt *c'* (4.5 M GuHCl, pH 7). The transient absorption difference spectrum measured immediately after CO dissociation ($t = 100$ ns) exhibits a broad feature in the Q-band region (530–570 nm) corresponding to a five-coordinate heme (^{H17}N) $\{^{Por}N_4Fe^{II}\}$. Subsequent absorption changes arise from the formation of a low-spin heme [$k_{obs} = 5(2) \times 10^4$ s^{-1}] before CO rebinding. Both experiments indicate that MS can bind to the heme in unfolded Fe^{II} -Cyt *c'* on the microsecond time scale (39–42).

Fe^{II} -Cyt *c'* Folding. Fe^{II} -Cyt *c'* folding was initiated by rapid electron injection (≈ 100 μs) into unfolded oxidized protein ([GuHCl] = 2.02–2.54 M) after two-photon laser excitation of NADH (43, 44). Under these conditions, heme reduction is slower than binding of the nonnative sixth ligand. The progress of the folding reaction was monitored by heme absorption in the Soret and Q-band regions from 10^{-4} to 1 s after excitation. The observed kinetics are highly heterogeneous. A small fraction ($\approx 20\%$) of the population forms a high-spin heme species in about a millisecond. Complete formation of the fully folded ensemble requires several seconds (Fig. 3). Rate constants for Fe^{II} -Cyt *c'* span a range from 10^3 to 10^{-1} s^{-1} revealing fast-folding (7.0×10^3 s^{-1} , 8%; 5.7×10^3 s^{-1} , 9%), intermediate-folding (9.0×10^2 to 1.5×10^1 s^{-1} , 24%), and slow-folding (5.9×10^{-1} s^{-1} , 16%; 4.8×10^{-1} s^{-1} , 43%) components in the protein ensemble (Fig. 3 *Inset*). Although the relative populations and the number of different rate constants vary slightly for kinetics measured at different wavelengths, heterogeneous behavior is always observed. On very long time scales, oxidation of the

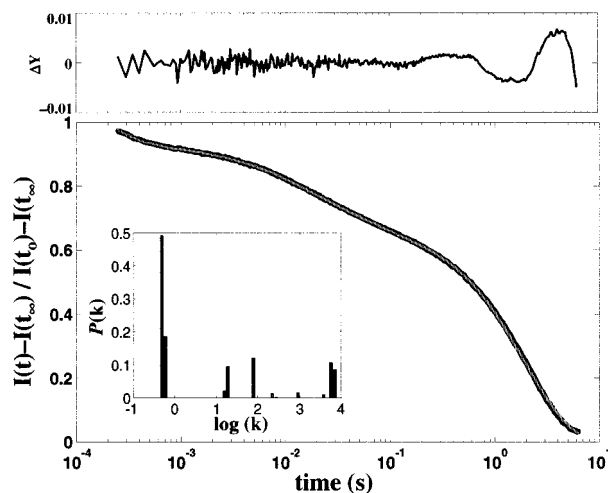


Fig. 3. Normalized folding kinetics (observed at 440 nm, black line) fit to 80 rate constants spanning logarithmically 10^5 to 10^{-2} s^{-1} (gray line) by using a non-negative least-squares algorithm. (*Upper*) Residuals from the fit. (*Inset*) The projected population of rate constants [7.0×10^3 s^{-1} (8%); 5.7×10^3 (9%); 9.2×10^2 (1%); 2.2×10^2 (1%); 7.9×10^1 (11%); 1.9×10^1 (9%); 1.5×10^1 (2%); 5.9×10^{-1} (16%); 4.8×10^{-1} (43%)].

reduced protein leads to some uncertainty in the extracted rate constants (although the samples were carefully deoxygenated, trace amounts of oxygen were always present). The transient difference spectrum recorded 100 μs after electron injection is characteristic of a mixture of five-coordinate, high-spin and six-coordinate, low-spin ferrohemes, suggesting that the slower folding populations are misligated. The difference spectra measured at 1 and 500 ms have been fit to a combination of the [(Fe^{II} -folded) – (Fe^{III} -unfolded)] and [(Fe^{II} -unfolded) – (Fe^{III} -unfolded)] molar difference spectra. The resulting folded and unfolded populations (1 ms, 25% folded, 75% unfolded; 500 ms, 52% folded, 48% unfolded) are consistent with the measured amplitude changes in the single wavelength kinetics.

Fe^{II} -Cyt *c'* Folding in the Presence of CO. To determine whether misligated heme traps are responsible for the slow Fe^{II} -Cyt *c'* folding, we examined ET-triggered folding of Fe^{II} -Cyt *c'* in the presence of CO. In the unfolded protein (3.32 M GuHCl, pH 7), CO binding occurs with a millisecond time constant [$1.0(4) \times 10^3$ s^{-1} ; 1 atm CO], whereas the folded protein binds CO much more slowly [$1.4(4)$ s^{-1}]. At lower denaturant concentration ([GuHCl] = 2.1 M, pH 7) in the presence of CO, reduction of unfolded Fe^{III} -Cyt *c'* is followed by two kinetics phases: a $1.4(6) \times 10^3$ s^{-1} step corresponding to CO binding, and $2.8(9)$ s^{-1} component due to $Fe^{II}(CO)$ -Cyt *c'* folding. The 1-ms transient difference spectrum can be modeled by two absorbing species: the major component is unfolded $Fe^{II}(CO)$ -Cyt *c'*, and the minor fraction is five-coordinate, folded Fe^{II} -Cyt *c'*. Subsequent changes in absorbance are associated with the conversion of unfolded $Fe^{II}(CO)$ - to folded $Fe^{II}(CO)$ -Cyt *c'* (Fig. 4).

Fe^{III} -Cyt *c'* Folding. Nonnative methionine-heme ligation is disfavored in unfolded Fe^{III} -Cyt *c'* (37), and the axial heme coordination sites are occupied by water and His-117. The stopped-flow triggered folding of Fe^{III} -Cyt *c'* is adequately described by a single kinetics phase with a rate constant that decreases exponentially with increasing denaturant concentration. The folding rate constant [$1.0(2)$ s^{-1} ; [GuHCl] = 0.95 M; $\Delta G_f = -16$ $kJ mol^{-1}$] is comparable to that of $Fe^{II}(CO)$ -Cyt *c'* and of the slower folding population of Fe^{II} -Cyt *c'* ([GuHCl] = 2.16 M; $\Delta G_f = -10$ $kJ mol^{-1}$). The extrapolated rate constant for folding

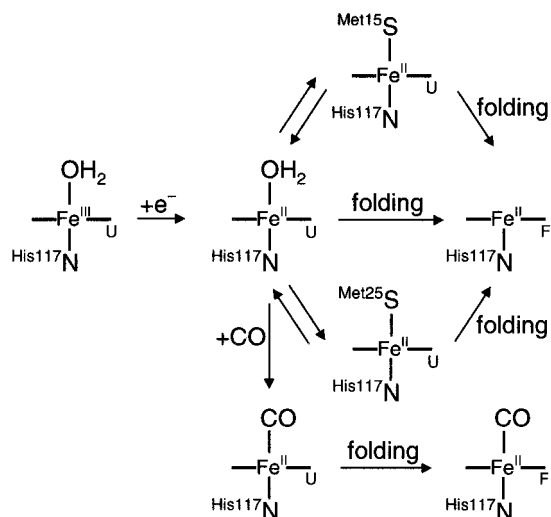


Fig. 4. Schematic representation of heme coordination environment after electron-transfer triggered folding of Fe^{II}-Cyt c' in the presence and absence of CO. The subscripts F and U refer to folded and unfolded polypeptides.

Fe^{III}-Cyt c' in the absence of denaturant is $2.5 \times 10^2 \text{ s}^{-1}$ [$\Delta G_f^\circ = -33(3) \text{ kJ mol}^{-1}$].

Discussion

It is reasonable to expect that topologically homologous proteins would fold at similar rates, yet cytochromes *b*₅₆₂ and *c'* display quite disparate folding kinetics. Apparently, there are factors beyond structural topology that must be considered to explain the folding kinetics of these four-helix bundles. Three key features of cytochromes *b*₅₆₂ and *c'* are likely to contribute to the differences in folding kinetics: covalent attachment of the porphyrin to the polypeptide, nonnative heme-ligand traps, and folding driving force.

The rapid dissociation of the heme from unfolded Fe^{II}-Cyt *b*₅₆₂ limits the time scale for observation of folding kinetics. Because the porphyrin is covalently attached in Fe-Cyt *c'*, the folding kinetics cover a far wider time range and are considerably more complex. A fraction of the unfolded Fe^{II}-Cyt *c'* ensemble refolds rapidly, but several seconds are required for the entire sample to fold. Proline isomerization is known to inhibit protein folding (45) but is unlikely to be responsible for the slow Fe-Cyt *c'* kinetics. Although there are four proline residues in the Cyt *c'* sequence, the observed folding rates depend on denaturant concentration and are substantially faster than typical proline isomerizations (45). It is interesting to note that the fast-folding fraction of Fe^{II}-Cyt *c'* is roughly comparable to the yield of folded Fe^{II}-Cyt *b*₅₆₂. It is possible, then, that if heme dissociation could be inhibited, Fe^{II}-Cyt *b*₅₆₂ would display slower and more complex folding kinetics.

The refolding of Fe^{II}-Cyt *c'* can be described qualitatively by a kinetic partitioning mechanism (46, 47). At the instant that folding is initiated, a fraction of the denatured proteins will have adopted conformations that can smoothly and rapidly fold to the native structure. The fast-folding population of Fe^{II}-Cyt *c'* would correspond to this group. Folding of the remaining fraction is frustrated by transient trapping in local minima on the folding energy landscape. Escape from these misfolded structures is an activated process that slows formation of the native structure. The partition factor that determines the balance between fast- and slow-folding populations depends on the primary sequence as well as the refolding conditions (46–51). Simulated folding kinetics of model three-helix-bundle proteins (48, 49) point to a central role for the folding free-energy gap in

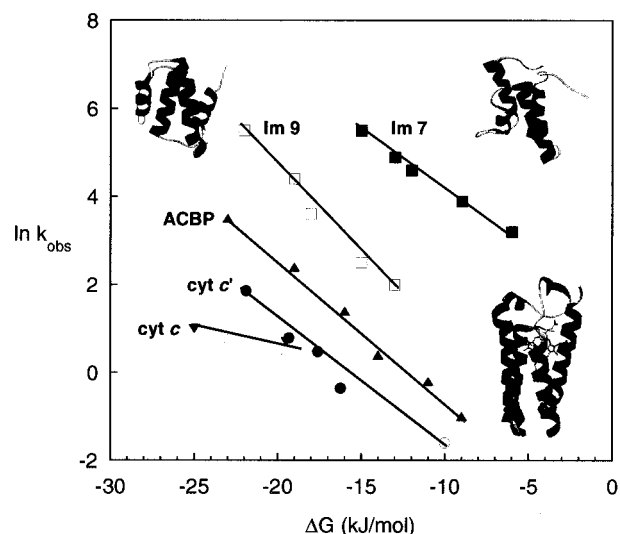


Fig. 5. Measured folding rates of helical proteins as functions of folding driving force (ΔG_f). Im7 (85 aa), pH 7, 10°C (■) (15); Im9 (85 aa) (PDB 1IMQ, upper right ribbon structure), pH 7, 10°C (□) (15); bovine ACBP (86 aa) (PDB 2ABD, upper left ribbon structure), pH 5.3, 5°C (▲) (12); Fe^{II}-Cyt c' (126 aa), pH 7, 22°C, slowest phase (○); Fe^{II}-Cyt c' (PDB 1A7V, lower right ribbon structure), pH 7, 22°C (●); equine Fe^{II}-Cyt c (104 aa), pH 7, 22°C (◇) (52); yeast Fe^{II}-Cyt c (108 aa), pH 7, 22°C (▼) (52).

determining the partitioning between fast- and slow-track folding. The heterogeneous folding kinetics of Fe^{II}-Cyt *c'* are strikingly similar to the simulated folding kinetics of a small-gap three-helix bundle (49).

Nonnative methionine ligands in unfolded Fe^{II}-Cyt *c'* contribute to the heterogeneity of the folding kinetics. In addition to the fast-folding population, there are intermediate ($\approx 10^2 \text{ s}^{-1}$) and slow-folding ($< 1 \text{ s}^{-1}$) components. Iron-sulfur bond dissociation is not rate limiting because ferroheme-methionine ligand exchange is faster than either folding phase (40). In the presence of CO, the nonnative Met ligands are displaced from the ferroheme, and folding is dominated by a slow phase with a time constant of $\approx 350 \text{ ms}$. Similarly, Fe^{III}-Cyt *c'* folding is not complicated by heme-ligand binding, and a single 1-s phase predominates. These observations suggest that, in the absence of misligation, Cyt *c'* requires 500 ms to 1 s to adopt a folded structure. The presence of an intermediate ($\approx 10^2 \text{ s}^{-1}$) folding phase in Fe^{II}-Cyt *c'* implies that nonnative methionine ligation can, in some instances, facilitate refolding. The protein has two Met residues that can bind to the ferroheme when the protein unfolds. It is possible that the intermediate phase arises from protein populations with $(^{\text{H117N}})\{\text{PorN}_4\text{Fe}^{\text{II}}\}(\text{M}^{15\text{S}})$ heme coordination, and the slow phase corresponds to populations with $(^{\text{H117N}})\{\text{PorN}_4\text{Fe}^{\text{II}}\}(\text{M}^{25\text{S}})$ ligation (Fig. 4). Met-15 is in the distal heme pocket in the folded protein, so an intermediate with $(^{\text{H117N}})\{\text{PorN}_4\text{Fe}^{\text{II}}\}(\text{M}^{15\text{S}})$ coordination might fold more readily than a $(^{\text{H117N}})\{\text{PorN}_4\text{Fe}^{\text{II}}\}(\text{M}^{25\text{S}})$ form.

The Fe-Cyt *c'* folding rates are compared in Fig. 5 to those of four structurally related proteins (11, 15, 19). The four-helix bundles Im7 and Im9 have 60% sequence identity and nearly identical three-dimensional structures, yet Im9 folds more than 10 times slower than Im7 (15). Curiously, Im9 displays the hallmarks of two-state folding, whereas intermediates are implicated in the faster Im7 folding process (15, 16). The folding of ACBP has been interpreted in terms of a two-state model (12, 13), although subsequent quenched-flow hydrogen exchange studies revealed that an intermediate is formed before the rate-limiting step (14). Among helical-bundle structures, there is a wide variation in measured folding rates as functions of $-\Delta G_f$

(Fig. 5). It is clear that, even in the absence of misligation, Cyt *c'* is the slowest folding protein in this structural class. The difference is even greater when account is taken of the fact that the Im7, Im9, and ACBP folding kinetics were measured at reduced temperatures. Cyt *c'* is substantially larger than the other helical bundles (Im7, 85 residues; Im9, 85 residues; ACBP, 86 residues; and Cyt *c'*, 126 residues), and its size may be in part responsible for its slower folding. On a free-energy basis, the Fe–Cyt *c'* folding kinetics more closely resemble those of Cyt *c* (52) than those of the nonheme helical-bundle proteins. Non-

native ligand binding clearly can perturb heme protein folding; it is likely that noncovalent, nonnative heme–polypeptide contacts represent additional sources of frustration.

We thank Michael Cusanovich and Terry Meyer (University of Arizona) for assistance with protein isolation and purification, Brian Crane for help with protein structure modeling, and Akif Tezcan for discussions. J.C.L. thanks the Ralph M. Parsons Foundation for a graduate fellowship. This work was supported by National Science Foundation Grant MCB-9974477 and by the Arnold and Mabel Beckman Foundation.

- Bryngelson, J. D., Onuchic, J. N. & Wolynes, P. G. (1995) *Proteins Struct. Funct. Genet.* **21**, 167–195.
- Onuchic, J. N., Lutheyschulten, Z. & Wolynes, P. G. (1997) *Annu. Rev. Phys. Chem.* **48**, 545–600.
- Dill, K. A. & Chan, H. S. (1997) *Nat. Struct. Biol.* **4**, 10–19.
- Plaxco, K. W., Simons, K. T. & Baker, D. (1998) *J. Mol. Biol.* **277**, 985–994.
- Plaxco, K. W., Simons, K. T., Ruczinski, I. & David, B. (2000) *Biochemistry* **39**, 11177–11183.
- Dinner, A. R. & Karplus, M. (2001) *Nat. Struct. Biol.* **8**, 21–22.
- Debe, D. A., Carlson, M. J. & Goddard, W. A., III (1999) *Proc. Natl. Acad. Sci. USA* **96**, 2596–2601.
- Muñoz, V. & Eaton, W. A. (1999) *Proc. Natl. Acad. Sci. USA* **96**, 11311–11316.
- Wittung-Stafshede, P., Gray, H. B. & Winkler, J. R. (1997) *J. Am. Chem. Soc.* **119**, 9562–9563.
- Wittung-Stafshede, P., Lee, J. C., Winkler, J. R. & Gray, H. B. (1999) *Proc. Natl. Acad. Sci. USA* **96**, 6587–6590.
- Kragelund, B. B., Robinson, C. V., Knudsen, J., Dobson, C. M. & Poulsen, F. M. (1995) *Biochemistry* **34**, 7217–7224.
- Kragelund, B. B., Højrup, P., Jensen, M. S., Schjerling, C. K., Juul, E., Knudsen, J. & Poulsen, F. M. (1996) *J. Mol. Biol.* **256**, 187–200.
- Kragelund, B. B., Osmark, P., Neergaard, T. B., Schiødt, J., Kristiansen, K., Knudsen, J. & Poulsen, F. M. (1999) *Nat. Struct. Biol.* **6**, 594–601.
- Teilum, K., Kragelund, B. B., Knudsen, J. & Poulsen, F. (2000) *J. Mol. Biol.* **301**, 1307–1314.
- Ferguson, N., Capaldi, A. P., James, R., Kleanthous, C. & Radford, S. E. (1999) *J. Mol. Biol.* **286**, 1597–1608.
- Capaldi, A. P., Shastry, M. C. R., Kleanthous, C., Roder, H. & Radford, S. E. (2001) *Nat. Struct. Biol.* **8**, 68–72.
- Huang, G. S. & Oas, T. G. (1995) *Proc. Natl. Acad. Sci. USA* **92**, 6878–6882.
- Pascher, T., Chesick, J. P., Winkler, J. R. & Gray, H. B. (1996) *Science* **271**, 1558–1560.
- Telford, J. R., Wittung-Stafshede, P., Gray, H. B. & Winkler, J. R. (1998) *Acc. Chem. Res.* **31**, 755–763.
- Meyer, T. E. & Kamen, M. D. (1982) *Adv. Protein Chem.* **35**, 105–212.
- Moore, G. R., McClune, G. J., Clayden, N. J., Williams, R. J. P., Alsaadi, B. M., Angstrom, J., Ambler, R. P., van Beeumen, J., Tempst, P., Bartsch, R. G., *et al.* (1982) *Eur. J. Biochem.* **123**, 73–80.
- Moore, G. R. & Pettigrew, G. W. (1990) *Cytochromes c: Evolutionary, Structural, and Physicochemical Aspects* (Springer, New York).
- Ambler, R. P., Bartsch, R. G., Daniel, M., Kamen, M. D., McLellan, L., Meyer, T. E. & Beeumen, J. V. (1981) *Proc. Natl. Acad. Sci. USA* **78**, 6854–6857.
- Hamada, K., Bethge, P. H. & Mathews, F. S. (1995) *J. Mol. Biol.* **247**, 947–962.
- Shibata, N., Iba, S., Misaki, S., Meyer, T. E., Bartsch, R. G., Cusanovich, M. A., Morimoto, Y., Higuchi, Y. & Yasuoka, N. (1998) *J. Mol. Biol.* **284**, 751–760.
- Moore, G. R., Williams, R. J. P., Peterson, J., Thomson, A. J. & Mathews, F. S. (1985) *Biochim. Biophys. Acta* **829**, 83–96.
- Klerk, H. D., Bartsch, R. G. & Kamen, M. D. (1965) *Biochim. Biophys. Acta* **97**, 275–280.
- Strekas, T. C. & Spiro, T. G. (1974) *Biochim. Biophys. Acta* **351**, 237–245.
- Fujii, S., Yoshimura, T., Kamada, H., Yamaguchi, K., Suzuki, S., Shidara, S. & Takakuwa, S. (1995) *BBA Protein Struct. Mol. Enzymol.* **1251**, 161–169.
- Clark, K., Dugad, L. B., Bartsch, R. G., Cusanovich, M. A. & Mar, G. N. L. (1996) *J. Am. Chem. Soc.* **118**, 4654–4664.
- Jackson, J. T., Mar, G. N. L. & Bartsch, R. G. (1983) *J. Biol. Chem.* **258**, 1799–1805.
- Barakat, R. & Strekas, T. C. (1982) *Biochim. Biophys. Acta* **679**, 393–399.
- Bartsch, R. G. (1971) *Methods Enzymol.* **23**, 344–363.
- Bartsch, R. G. (1978) in *The Photosynthetic Bacteria*, eds. Clayton, R. K. & Sistrom, W. R. (Plenum, New York), pp. 249–279.
- Nozaki, Y. (1972) *Methods Enzymol.* **26**, 43–50.
- Stowell, M. H. B., Larsen, R. W., Winkler, J. R., Rees, D. C. & Chan, S. I. (1993) *J. Phys. Chem.* **97**, 3054–3057.
- Tezcan, F. A., Winkler, J. R. & Gray, H. B. (1998) *J. Am. Chem. Soc.* **120**, 13383–13388.
- Bren, K. L. & Gray, H. B. (1993) *J. Am. Chem. Soc.* **115**, 10382–10383.
- Hagen, S. J., Hofrichter, J., Szabo, A. & Eaton, W. A. (1996) *Proc. Natl. Acad. Sci. USA* **93**, 11615–11617.
- Hagen, S. J., Hofrichter, J. & Eaton, W. A. (1997) *J. Phys. Chem.* **101**, 2352–2365.
- Lapidus, L. J., Eaton, W. A. & Hofrichter, J. (2000) *Proc. Natl. Acad. Sci. USA* **97**, 7220–7225.
- Hagen, S. J., Carswell, C. W. & Sjolander, E. M. (2001) *J. Mol. Biol.* **305**, 1161–1171.
- Telford, J. R., Tezcan, F. A., Gray, H. B. & Winkler, J. R. (1999) *Biochemistry* **38**, 1944–1949.
- Orii, Y. (1993) *Biochemistry* **32**, 11910–11911.
- Schmid, F. X., Mayr, L. M., Mücke, M. & Schönbrunner, E. R. (1993) *Adv. Protein Chem.* **44**, 25–66.
- Thirumalai, D., Klimov, D. K. & Woodson, S. A. (1997) *Theor. Chem. Acc.* **96**, 14–22.
- Thirumalai, D. & Klimov, D. K. (1999) *Curr. Opin. Struct. Biol.* **9**, 197–207.
- Zhou, Y. & Karplus, M. (1999) *Nature (London)* **401**, 400–403.
- Zhou, Y. & Karplus, M. (1999) *J. Mol. Biol.* **293**, 917–951.
- Shea, J.-E., Onuchic, J. N. & Brooks, C. L., III (2000) *J. Chem. Phys.* **113**, 7663–7671.
- Shea, J.-E., Onuchic, J. N. & Brooks, C. L., III (1999) *Proc. Natl. Acad. Sci. USA* **96**, 12512–12517.
- Mines, G. A., Pascher, T., Lee, S. C., Winkler, J. R. & Gray, H. B. (1996) *Chem. Biol.* **3**, 491–497.